Robust Linearly Constrained Filtering for GNSS Position and Attitude Estimation under Antenna Baseline Mismatch

Paul Chauchat
ISAE-SUPAERO
University of Toulouse
Toulouse, France
paul.chauchat@isae.fr

Daniel Medina
Institute of Comm. and Nav.
German Aerospace Center (DLR)
Neustrelitz, Germany
daniel.ariasmedina@dlr.de

Jordi Vilà-Valls
ISAE-SUPAERO
University of Toulouse
Toulouse, France
jordi.vila-valls@isae.fr

Eric Chaumette
ISAE-SUPAERO
University of Toulouse
Toulouse, France
eric.chaumette@isae.fr

***Abstract*—Precise navigation solutions are fundamental for new intelligent transportation systems and robotics applications, where attitude also plays an important role. Among the different technologies available, Global Navigation Satellite Systems (GNSS) are the main source of positioning data. In the GNSS context, carrier phase observations are mandatory to obtain precise positioning, and multiple antenna setups must be considered for attitude determination. Position and attitude estimation have been traditionally tackled in a separate manner within the GNSS community, but a recently introduced recursive joint position and attitude (JPA) Kalman filter-like approach has shown the potential benefits of the joint estimation. One of the drawbacks of the original JPA is the assumption of perfect system knowledge, and in particular the baseline distance between antennas, which may not be the case in real-life applications and can lead to a severe performance degradation. The goal of this contribution is to propose a robust filtering approach able to mitigate the impact of a possible GNSS antenna baseline mismatch, exploiting the use of linear constraints. Illustrative results are provided to support the discussion and show the performance improvement, for both GNSS-based attitude-only and JPA estimation.**

***Index Terms*—GNSS, position and attitude estimation, robust filtering, model mismatch, linear constraints.**

I. Introduction

It is well known that Global Navigation Satellite Systems (GNSS) have become the cornerstone source of positioning data, and this dependence can only but grow in the future [1]. It is commonly said that "GNSS are everywhere", a thought-provocative statement which refers to the huge variety of mass-market, safety-critical, civil and military applications, within a plethora of engineering fields, where reliable, continuous and precise positioning information is nowadays of paramount importance. In addition of being the position-related information technology of choice, GNSS are also fundamental for timing applications, and if using multiple antenna setups they can also be exploited for attitude estimation. The latter is of particular interest in aerospace, for satellite orbit determination [2]–[4], and outdoor navigation in vehicular and robotics applications [5]–[7].

Standard GNSS receivers resort to a multilateration procedure, where a set of code (delay) and Doppler measurements are fused to estimate the receiver position and velocity, as well as the receiver clock offset and drift. Such solution can be obtained in a snapshot manner using least squares (LS)-type methods [8], or in a recursive way using Kalman filter (KF)-like techniques [1, Ch. 22]. In order to obtain a precise positioning solution (i.e., sub-decimeter precision), carrier phase measurements must be exploited, which in turn implies the challenging estimation of a set of integer ambiguities, widely known as ambiguity resolution (AR). This is the case for instance in Real Time Kinematic (RTK) differential positioning. Again, both LS-type [1, Chap 26] or KF-based approaches [9] exist in the literature. In both cases, integer ambiguities are typically estimated with a so-called Integer LS (ILS) [10].

In addition to precise navigation, GNSS carrier phase measurements can also be exploited for attitude determination, which refers to the estimation of a moving rigid body orientation with respect to (w.r.t.) its environment [11]. Indeed, considering a multi-antenna GNSS system, the goal is to estimate the rotation which relates the baseline vectors joining each pair of antenna positions across two frames of interest. The most popular GNSS attitude estimation method is the so-called MC-LAMBDA [12]. Attitude estimation has been traditionally decoupled from position estimation, and only addressed in a snapshot manner, but in practice the recursive joint position and attitude (JPA) estimation is of interest. A recursive JPA KF-based solution was recently proposed in [13] to correctly cope with the cross-correlation between the positioning- and attitude-related observations. The main drawback of this approach is that a perfect system knowledge is considered, i.e., a perfectly surveyed distance between antennas. In real-life applications, such antenna baseline may be misspecified for several reasons, which may induce a significant performance degradation, therefore, robust solutions must be accounted for.

Within the GNSS-based attitude and JPA estimation context,

This work has been partially supported by the French DGA/AID under projects 2018.60.0072.00.470.75.01 and 2019.65.0068.00.470.75.01, and the Agence Nationale de la Recherche project ANR-17-CE22-0001-01.

the goal of this contribution is to propose a robust KF-based filtering approach able to mitigate the impact of a possible antenna baseline mismatch (i.e., system model mismatch). The idea is to resort to linear constraints to mitigate the mismatch, that is, using the recently introduced linearly constrained extended KF [14], [15]. Illustrative results are provided to support the discussion and show the performance improvement w.r.t. state-of-the-art solutions, for both GNSS-based attitude-only and JPA estimation.

II. GNSS-Based Precise Position and Attitude Estimation

In the following, the navigation problem for a vehicle equipped with multiple GNSS antennas is addressed. In particular, we are interested in exploiting GNSS code and carrier phase observations for obtaining precise position and attitude estimates.

A. Recursive Estimation for the Navigation Problem

Considering a discrete state-space (DSS) model, the state vector for the navigation problem can be described by

$$\begin{aligned} \mathbf{x}_k^\top &= \left[\mathbf{q}_k^\top, \mathbf{a}_k^\top, \mathbf{b}_k^\top\right], \\ \text{with } &(\mathbf{q}_k, \mathbf{a}_k, \mathbf{b}_k) \in \mathcal{S}^3 \times \mathbb{Z}^M \times \mathbb{R}^L, \end{aligned} \tag{1}$$

where $\mathbf{q}_k$ denotes the unit quaternion rotation from the body to the (global) navigation frame –denoted with subscripts $\mathcal{B}$ and $\mathcal{G}$ respectively–, $\mathbf{a}_k$ is the vector of carrier phase integer ambiguities, and $\mathbf{b}_k$ is a vector comprising the remaining L real-valued unknown parameters. This work analyzes two applications:

i) Attitude estimation with gyroscope integration. In this case, the gyroscope biases are estimated $\mathbf{b} = \mathbf{b}_\omega, L = 3$ and the number of ambiguities is $M = n \cdot N$, with $n+1$ GNSS tracked satellites over $N+1$ antennas installed on the vehicle.

ii) JPA estimation with gyroscope integration. In addition to the gyroscope biases, and the vectors of position (w.r.t. the base station) and velocity are included in $\mathbf{b}$: $\mathbf{b}^\top = [\mathbf{b}_\omega{}^\top, \mathbf{p}^\top, \mathbf{v}^\top], L = 9$, and the integer ambiguities are of dimension $M = n \cdot (N+1)$.

The dimension of the vector of ambiguities directly comes from the use of double differences in the measurement model, as recalled in Section II-C, and detailed in [13].

Recursive estimation for the previous DSS is typically addressed via KF, which allows modeling the evolution of the states over time, through a *process model* $\mathbf{f}(\cdot)$, and the relationship of these to the observations, through an *observation model* $\mathbf{h}(\cdot)$, as

$$\mathbf{x}_k = \mathbf{f}\left(\mathbf{x}_{k-1}, \boldsymbol{\omega}_{k-1}, \mathbf{w}_{k-1}\right), \tag{2}$$

$$\mathbf{y}_k = \mathbf{h}\left(\mathbf{x}_k, \boldsymbol{\theta}_k\right) + \boldsymbol{\eta}_k, \tag{3}$$

$\boldsymbol{\omega}_{k-1}$ is a given input, and $\mathbf{w}_{k-1} \sim \mathcal{N}(\mathbf{0}, \mathbf{Q}_{k-1})$ the process noise vector. Here, in both attitude-only and JPA cases, $\boldsymbol{\omega}_{k-1}$ is a set of gyroscope readings. The full process-model is detailed in Section II-B. The measurement function $\mathbf{h}(\cdot)$ relates the GNSS observations (i.e., the code and carrier phase pseudoranges tracked over the antennas on the body frame and, for JPA, also for the base station) to the state estimate, as detailed in Section II-C, and of known noise distribution $\boldsymbol{\eta}_k \sim \mathcal{N}(\mathbf{0}, \boldsymbol{\Sigma}_k)$. The measurement function is conditioned on a set of known parameters $\boldsymbol{\theta}_k$, in this case the inter-antenna baseline vectors, measured in the local vehicle frame. For nonlinear models, as for (2)-(3), the time recursion estimation is commonly addressed with a nonlinear KF formulation.

Recursive attitude estimation must also take into account and respect its inherent non-linear geometric constraints – either the orthogonality and unit determinant for the rotation matrix or the unit norm for the quaternion– [16], [17]. This is now a well-known problem, typically addressed by geometric tools such as Lie group theory [18]. This work considers the Error State KF (ESKF) –also known as Indirect KF– [19], [20], for which the state to be estimated $\mathbf{x}$ belongs to a manifold and its perturbations $\delta\mathbf{x}$ "live" in the tangent space of that manifold. Thus, the unknown true state is formulated as the composition of the nominal estimate $\hat{\mathbf{x}}$ and the error state $\delta\mathbf{x}$, noted $\mathbf{x} = \widehat{\mathbf{x}} \oplus \delta\mathbf{x}$, and defined by (6), with the error state described by

$$\begin{aligned} \delta\mathbf{x}_k^\top &= \left[\delta\boldsymbol{\psi}_k^\top, \delta\mathbf{a}_k^\top, \delta\mathbf{b}_k^\top\right], \\ \text{with } &(\delta\boldsymbol{\psi}_k, \delta\mathbf{a}_k, \delta\mathbf{b}_k) \in \mathbb{R}^3 \times \mathbb{R}^M \times \mathbb{R}^L, \end{aligned} \tag{4}$$

and $\delta\boldsymbol{\psi}_k$ the rotation vector. The Euclidean space for $\delta\boldsymbol{\psi}_k$ connects to the Lie algebra $\mathbf{u}\varphi \in \mathfrak{s}^3$ (with $\mathbf{u}$ an unit vector of rotation and φ the rotated angle) with the isomorphism $(\cdot)^\wedge : \mathbb{R}^3 \mapsto \mathfrak{s}^3$. Then, the Lie algebra connects with $\mathcal{S}^3$ through exponential mapping. The overall procedure is given by

$$\delta\boldsymbol{\psi} \in \mathbb{R}^3 \xmapsto{(\cdot)^\wedge} \mathbf{u}\varphi \in \mathfrak{s}^3 \xmapsto{\exp(\cdot)} \delta\mathbf{q} \in \mathcal{S}^3, \tag{5}$$

$$(\delta\boldsymbol{\psi})^\wedge : \begin{cases} \mathbf{u} = \frac{\delta\boldsymbol{\psi}}{\|\delta\boldsymbol{\psi}\|^2} \\ \varphi = \|\delta\boldsymbol{\psi}\|^2 \end{cases}, \exp(\mathbf{u}\varphi) : \begin{bmatrix} \cos(\varphi/2) \\ \mathbf{u}\sin(\varphi/2) \end{bmatrix}.$$

In a compact expression, the composition of nominal and error state is as follows

$$\mathbf{x} = \widehat{\mathbf{x}} \oplus \delta\mathbf{x} = \begin{cases} \widehat{\mathbf{q}}_k & \circ & \delta\mathbf{q}_k \\ \widehat{\mathbf{a}}_k & + & \delta\mathbf{a}_k \\ \widehat{\mathbf{b}}_k & + & \delta\mathbf{b}_k \end{cases}, \tag{6}$$

with $\circ$ the quaternion product. For a more detailed discussion on Lie group theory, please refer to [18], [21], [22].

The ESKF adapts the EKF framework to a chosen non-linear parametrisation, here given by (6) to preserve the unit-norm quaternion constraint, while using a minimal parametrisation of the covariance matrix. That is, it uses the $\oplus$ operator, instead of the standard addition, to linearise and update the system. Let $\widehat{\mathbf{x}}_{k-1|k-1}$ denote the estimate at step $k-1$, and $\mathbf{P}_{k-1|k-1}$ its estimated covariance. Then the propagation and update steps

of the ESKF are given by

$$\widehat{\mathbf{x}}_{k|k-1} = \mathbf{f}(\widehat{\mathbf{x}}_{k-1|k-1}, \boldsymbol{\omega}_{k-1}) \tag{7a}$$
$$\mathbf{P}_{k|k-1} = \mathbf{F}_{k-1}\mathbf{P}_{k-1|k-1}\mathbf{F}_{k-1}^{\top} + \mathbf{Q}_{k-1}, \tag{7b}$$
$$\mathbf{S}_k = \mathbf{H}_k\mathbf{P}_{k|k-1}\mathbf{H}_k^{\top} + \boldsymbol{\Sigma}_k, \tag{7c}$$
$$\mathbf{K}_k = \mathbf{P}_{k|k-1}\mathbf{H}_k^{\top}\mathbf{S}_k^{-1}, \tag{7d}$$
$$\widehat{\mathbf{x}}_{k|k} = \widehat{\mathbf{x}}_{k|k-1} \oplus \mathbf{K}_k(\mathbf{y}_k - \mathbf{h}(\widehat{\mathbf{x}}_{k|k-1}, \boldsymbol{\theta})), \tag{7e}$$
$$\mathbf{P}_{k|k} = (\mathbf{I} - \mathbf{K}_k\mathbf{H}_k)\mathbf{P}_{k|k-1}. \tag{7f}$$

The matrices $\mathbf{F}_{k-1}, \mathbf{H}_k$ are the Jacobians of $\mathbf{f}, \mathbf{h}$ with respect to $\oplus$, which can be computed by the chain rule as

$$\begin{aligned}\mathbf{F}_{k-1} &= \left.\frac{\partial \mathbf{f}(\mathbf{x} \oplus \delta\mathbf{x}, \boldsymbol{\omega}_{k-1})}{\partial \delta\mathbf{x}}\right|_{\widehat{\mathbf{x}}_{k-1|k-1}, \boldsymbol{\omega}_{k-1}} \\ &= \left.\frac{\partial \mathbf{f}}{\partial \mathbf{x}}\right|_{\widehat{\mathbf{x}}_{k|k-1}, \boldsymbol{\omega}_{k-1}} \left.\frac{\partial \mathbf{x} \oplus \delta\mathbf{x}}{\partial \delta\mathbf{x}}\right|_{\widehat{\mathbf{x}}_{k-1|k-1}}\end{aligned} \tag{8}$$

$$\begin{aligned}\mathbf{H}_k &= \left.\frac{\partial \mathbf{h}(\mathbf{x} \oplus \delta\mathbf{x}, \boldsymbol{\theta})}{\partial \delta\mathbf{x}}\right|_{\widehat{\mathbf{x}}_{k|k-1}, \boldsymbol{\theta}} \\ &= \left.\frac{\partial \mathbf{h}}{\partial \mathbf{x}}\right|_{\widehat{\mathbf{x}}_{k|k-1}, \boldsymbol{\theta}} \left.\frac{\partial \mathbf{x} \oplus \delta\mathbf{x}}{\partial \delta\mathbf{x}}\right|_{\widehat{\mathbf{x}}_{k|k-1}}\end{aligned} \tag{9}$$

Hereinafter, the dynamics and the observation models are detailed.

B. Constant-Speed Model with a Gyroscope

A typical dynamical model regards a vehicle to move according to the constant-velocity non-turning model [23], which was the one considered initially for JPA [13]. Because of the limitations of a non-turning model, we extend JPA to systems equipped with a gyroscope. Indeed, gyroscopes allow tracking fast and more complex rotations, and are typically equipped in a growing number of applications [24]. Since accelerometers are not strictly required for attitude determination, this work disregards its use. Most gyroscopes are subject to an inherent and slowly varying bias, which needs to be estimated online, and was thus included in (1). Moreover, the ambiguities are assumed time invariant in the absence of cycle slip occurrence. The constant-speed model then writes, for JPA and without noise

$$\mathbf{f}(\mathbf{x}_{k-1}, \boldsymbol{\omega}_{k-1}) = \begin{cases} \mathbf{q}_{k-1} \circ \boldsymbol{\Omega}_{k-1} \\ \mathbf{a}_{k-1} \\ \mathbf{b}^{\omega}_{k-1} \\ \mathbf{p}_{k-1} + dt\ \mathbf{v}_{k-1} \\ \mathbf{v}_{k-1} \end{cases} \tag{10}$$
$$\text{with } \boldsymbol{\Omega}_{k-1} = \exp((\boldsymbol{\omega}_{k-1} - \mathbf{b}^{\omega}_{k-1})^{\wedge}).$$

using (5) to define $\boldsymbol{\Omega}_k$. Notice that, for case i) of attitude-only estimation, it is exactly the same, simply without the position and velocity lines. Thus, the associated Jacobians are easily obtained, in both cases of attitude-only and JPA estimation

$$\mathbf{F}_k^{\text{att}} = \begin{bmatrix} \boldsymbol{\Omega}_k^{\top} & & -dt\mathbf{I}_3 \\ & \mathbf{I}_M & \\ & & \mathbf{I}_3 \end{bmatrix}, \mathbf{F}_k^{\text{JPA}} = \begin{bmatrix} \mathbf{F}_k^{\text{att}} & & \\ & \mathbf{I}_3 & dt\mathbf{I}_3 \\ & & \mathbf{I}_3 \end{bmatrix}.$$

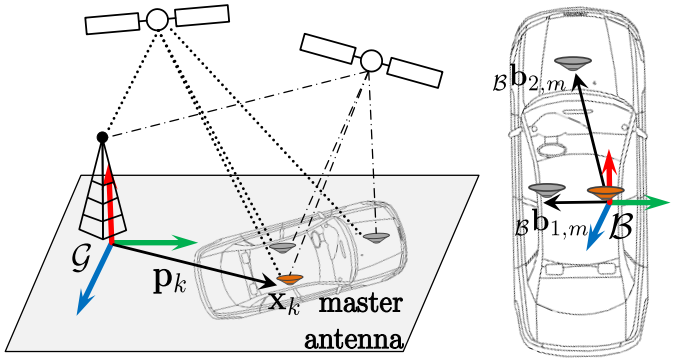

Fig. 1. On the left, illustration for the GNSS-based JPA problem: the base station, the rover with multiple antennas. On the right, the configuration of the sensors on the body frame. The master antenna is highlighted in orange color.

C. GNSS-Based Position and Attitude Observation Model

Consider a vehicle equipped with $N+1$ antennas and receiving corrections from a nearby base station of known location, as illustrated in Fig. 1. In multi-antenna platforms, one of the antennas is considered as *master* and center of the local body frame, and the remaining antennas are denoted as *slaves*. The global frame $\mathcal{G}$ is typically centered on the base station location. To eliminate atmospheric delays and other nuisance parameters, the "original" undifferenced GNSS measurements at the base and slaves antennas are mixed with those of the master antenna using the double difference (DD) combination [13, Sec. 3]. The DD code and carrier phase combinations constitute the positioning- and attitude-related observations. The subscripts m, b, and $j = 1, \ldots, N$ refer to the GNSS measurements for the master, base and slaves antennas respectively. For simplicity, in the remaining of this Section the time index k is dropped.

a) Position-related observations: These observations, noted $\mathbf{y}_{\text{pos}}$, are described as

$$\mathbf{y}_{\text{pos}} = \begin{bmatrix} \boldsymbol{\Phi}_{b,m} \\ \boldsymbol{\rho}_{b,m} \end{bmatrix}, \ \boldsymbol{\Phi}_{b,m}, \boldsymbol{\rho}_{b,m} \in \mathbb{R}^n, \tag{11a}$$
$$[\boldsymbol{\Phi}_{b,m}]_i = -\mathbf{u}_i^{\top}\mathbf{p}_k + \lambda \cdot a_{r_i} + \epsilon_{b,m_i}, \tag{11b}$$
$$[\boldsymbol{\rho}_{b,m}]_i = -\mathbf{u}_i^{\top}\mathbf{p}_k + \varepsilon_{b,m_i}, \tag{11c}$$

with $\boldsymbol{\rho}$ and $\boldsymbol{\Phi}$ the vector of DD code and carrier phase observations, $[\boldsymbol{\alpha}]_i$ and/or α_i denote the i-th coordinate of a generic vector $\boldsymbol{\alpha}$, $\mathbf{u}_i$ is the DD line-of-sight satellite steering vector, λ is the GNSS carrier wavelength and $\epsilon_{b,m_i}, \varepsilon_{b,m_i}$ indicate the carrier phase and code noises for the i-th observation ($i = 1, \ldots, n$). The subscript r_i in (11b) refers to the ambiguity associated with the i-th DD observation between the base station and master antennas.

b) Attitude-related observations: Their vector of observations, denoted $\mathbf{y}_{\text{att}}$, is as follows

$$\mathbf{y}_{\text{att}}^\top = \left[\boldsymbol{\Phi}_{1,m}^\top, \dots, \boldsymbol{\Phi}_{N,m}^\top, \boldsymbol{\rho}_{1,m}^\top, \dots, \boldsymbol{\rho}_{N,m}^\top\right], \quad \text{with } \boldsymbol{\Phi}_{j,m}, \boldsymbol{\rho}_{j,m} \in \mathbb{R}^n, j = 1, \dots, N. \tag{12a}$$

$$[\boldsymbol{\Phi}_{j,m}]_i = -\mathbf{u}_i^\top \mathbf{R}(\mathbf{q})_{\mathcal{B}}\mathbf{b}_{j,m} + \lambda \cdot a_{r_j,i} + \epsilon_{j,m_i}, \tag{12b}$$

$$[\boldsymbol{\rho}_{j,m}]_i = -\mathbf{u}_i^\top \mathbf{R}(\mathbf{q})_{\mathcal{B}}\mathbf{b}_{j,m} + \varepsilon_{j,m_i}, \tag{12c}$$

where $\mathbf{R}(\mathbf{q})$ is the rotation matrix from the body frame $\mathcal{B}$ to the global navigation frame $\mathcal{G}$, derived from the associated quaternion, and ${}_{\mathcal{B}}\mathbf{b}_{j,m}$ denotes the baseline vector between the j-th slave and master antennas, measured in the body frame $\mathcal{B}$ of the vehicle. The subscript r_j, i in (12b) refers to the ambiguity associated with the i-th DD observation between the j-th slave and master antennas. Based on the two study cases, attitude-only and JPA estimation, the vector of observations consists on $\mathbf{y} = \mathbf{y}_{\text{att}}$ and $\mathbf{y}^\top = \left[\mathbf{y}_{\text{pos}}^\top, \ \mathbf{y}_{\text{att}}^\top\right]$, respectively and the associated covariance matrix $\boldsymbol{\Sigma}$ is as defined in [13]. The inter-antenna baselines in the local frame $\mathcal{B}$ constitute the parameters $\boldsymbol{\theta}$, on which the observation model is dependent:

$$\boldsymbol{\theta} = \left[{}_{\mathcal{B}}\mathbf{b}_{1,m}^\top, \dots, {}_{\mathcal{B}}\mathbf{b}_{N,m}^\top\right]^\top. \tag{13}$$

III. Linearly Constrained Filtering

A. Mismatch-Induced Bias

As explained in Section II-A, standard filtering techniques rely on models of the considered system (2), (3). The observation models involves some parameters $\boldsymbol{\theta}_k$, and, in general, the process model might also show such a dependency to parameters $\boldsymbol{\xi}_{k-1}$. In theory, both are supposed to be known. In practice, one might only have approximate, or assumed, values of $\boldsymbol{\xi}_{k-1}, \boldsymbol{\theta}_k$, denoted as $\widehat{\boldsymbol{\xi}}_{k-1}, \widehat{\boldsymbol{\theta}}_k$. The difference between the true and assumed models can be expressed as $d\boldsymbol{\xi}_{k-1} = \boldsymbol{\xi}_{k-1} - \widehat{\boldsymbol{\xi}}_{k-1}$ and $d\boldsymbol{\theta}_k = \boldsymbol{\theta}_k - \widehat{\boldsymbol{\theta}}_k$, which we do not try to estimate: either i) to keep the system's dimension low, ii) because we have no adequate prior distribution for its value, or iii) because we have no adequate model of its evolution. Since the systems which are considered in this paper use constant velocity models, no mismatch is present on the evolution, so that $d\boldsymbol{\xi}_{k-1} = \mathbf{0}$.

Assuming that the mismatch $d\boldsymbol{\theta}_k$ is small enough, one can carry a first-order expansion to study its impact on the estimation. We thus have

$$\mathbf{y}_k \simeq \underbrace{\mathbf{h}(\mathbf{x}_k, \widehat{\boldsymbol{\theta}}_k)}_{\widehat{\mathbf{y}}_k} + \left.\frac{\partial \mathbf{h}}{\partial \boldsymbol{\theta}}\right|_{\mathbf{x}_k, \widehat{\boldsymbol{\theta}}_k} d\boldsymbol{\theta}_k \tag{14}$$

Consider an EKF devised to estimate $\mathbf{x}$ from (2), (3) but with the assumed parameter $\widehat{\boldsymbol{\theta}}_k$. Denote its estimate as $\widehat{\mathbf{x}}_{k|k-1}$ after the prediction, and as $\widehat{\mathbf{x}}_{k|k}(\mathbf{L})$ after an update step using a gain $\mathbf{L}$. In addition, let the error be $\mathbf{e} = \widehat{\mathbf{x}} - \mathbf{x}$. Then, it becomes after the update

$$\mathbf{e}_{k|k} = \widehat{\mathbf{x}}_{k|k}(\mathbf{L}) - \mathbf{x}_k = \widehat{\mathbf{x}}_{k|k-1} - \mathbf{x}_k + \mathbf{L}_k(\mathbf{h}(\mathbf{x}_k, \boldsymbol{\theta}_k) + \mathbf{v}_k - \mathbf{h}(\widehat{\mathbf{x}}_{k|k-1}, \widehat{\boldsymbol{\theta}}_k))$$

In the standard EKF methodology, a first-order expansion of $\mathbf{h}$ and $\mathbf{f}$ with respect to $\mathbf{x}$ is carried out to determine the appropriate gain. However, here, the difference between $\mathbf{h}(\mathbf{x}_k, \boldsymbol{\theta}_k)$ and $\mathbf{h}(\widehat{\mathbf{x}}_{k|k-1}, \widehat{\boldsymbol{\theta}}_k)$ would not boil down to a term involving $\mathbf{e}_{k|k-1}$ due to the mismatch. Thus, expansions both with respect to $\mathbf{x}$ and $\boldsymbol{\theta}$ must be carried out, computed at $\widehat{\mathbf{x}}_{k|k-1}$ and $\widehat{\boldsymbol{\theta}}_k$. Indeed, we have

$$\mathbf{e}_{k|k} = \mathbf{e}_{k|k-1} + \mathbf{L}\mathbf{v}_k + \mathbf{L}(\mathbf{h}(\mathbf{x}_k, \boldsymbol{\theta}_k) - \mathbf{h}(\widehat{\mathbf{x}}_k, \widehat{\boldsymbol{\theta}}_k)) \tag{15a}$$

Thus, neglecting the cross derivatives in $\mathbf{x}$ and $\boldsymbol{\theta}$, and noting $\widehat{\mathbf{H}}_k = \frac{\partial \mathbf{h}}{\partial \mathbf{x}}\big|_{\widehat{x}_k, \widehat{\boldsymbol{\theta}}_k}$, this leads to

$$\mathbf{e}_{k|k} \simeq (\mathbf{I} - \mathbf{L}\widehat{\mathbf{H}}_k)\mathbf{e}_{k|k-1} + \mathbf{L}\mathbf{v}_k + \underbrace{\mathbf{L}\left.\frac{\partial \mathbf{h}}{\partial \boldsymbol{\theta}}\right|_{\mathbf{x}_k, \widehat{\boldsymbol{\theta}}_k} d\boldsymbol{\theta}_k}_{\varepsilon_k(\mathbf{L})}, \tag{15b}$$

It thus appears that the mismatch induces an additional bias term $\boldsymbol{\varepsilon}_k(\mathbf{L})$, which will not be corrected by the subsequent filtering steps.

B. Mitigating the Mismatch: the LCEKF Methodology

In order to mitigate the bias induced by the model mismatch, it was recently proposed to choose the gain $\mathbf{L}$ in order to cancel out the uncontrolled error: $\boldsymbol{\varepsilon}_k(\mathbf{L}) = \mathbf{0}$, so that (15b) falls down to its well-known form. We can then minimize the filter MSE, but only under this constraint. This yields the linearly constrained Extended KF (LCEKF) [14], [15]. We briefly recall here the methodology, specifying it for the problem we consider (in particular, no mismatch on the process model). Since it focuses on the linearised system, it is not affected by the parametrisation of the state, and can thus be seamlessly applied to the ESKF.

The goal is to cancel the bias for any value of the mismatch $d\boldsymbol{\theta}_k$, as long as the Taylor expansion holds. However, since the true state $\mathbf{x}_k$ is unknown, the partial derivative must be approximated at $\widehat{\mathbf{x}}_{k|k-1}$ [14]. Thus, the gain is chosen as that of the standard EKF, but with constraints, according to

$$\mathbf{L}_k = \underset{\mathbf{L}}{\operatorname{argmin}} \left\{\mathbb{E}\left[\mathbf{e}_{k|k}\mathbf{e}_{k|k}^\top\right]\right\} \quad \text{s.t. } \mathbf{L}\boldsymbol{\Delta}_k = \mathbf{0}, \quad \boldsymbol{\Delta}_k = \left.\frac{\partial \mathbf{h}}{\partial \boldsymbol{\theta}}\right|_{\widehat{\mathbf{x}}_{k|k-1}, \widehat{\boldsymbol{\theta}}_k} \tag{16}$$

Considered on the linearised system (15b), this constrained optimisation problem has a closed form, which is given by [14]

$$\mathbf{L}_k = \mathbf{K}_k(\mathbf{I} - \boldsymbol{\Delta}_k \boldsymbol{\Psi}_k^{-1} \boldsymbol{\Delta}_k^\top \left(\mathbf{S}_{k|k-1}\right)^{-1}) \tag{17}$$

where $\mathbf{K}_k$ is the unconstrained gain of the EKF, which is given along with $\mathbf{S}_{k|k-1}$ by (7d)-(7c), and $\boldsymbol{\Psi}_k = \boldsymbol{\Delta}_k^\top (\mathbf{S}_{k|k-1})^{-1} \boldsymbol{\Delta}_k$. Using this modified gain also impacts how the covariance is updated. It is now obtained as

$$\mathbf{P}_{k|k} = (\mathbf{I} - \mathbf{K}_k \widehat{\mathbf{H}}_k)\mathbf{P}_{k|k-1} + \mathbf{K}_k \boldsymbol{\Delta}_k \boldsymbol{\Psi}_k^{-1} \boldsymbol{\Delta}_k^\top \mathbf{K}_k^\top \tag{18}$$

Note that the constraint needs to be feasible, i.e., $\boldsymbol{\Delta}_k$ must be of size $N_k \times s_k$, with $s_k < N_k$, and of rank s_k. Similarly, the updated state estimate reads

$$\widehat{\mathbf{x}}_{k|k} = \widehat{\mathbf{x}}_{k|k-1} + \mathbf{L}_k(\mathbf{y}_k - \mathbf{h}(\widehat{\mathbf{x}}_{k|k-1}, \widehat{\boldsymbol{\theta}}_k)), \tag{19}$$

for a general form. In the following, we particularize the aforedescribed linearly constrained filter for the attitude and JPA problems estimated via an ESKF.

C. Application to the Attitude-only and JPA Problems

The GNSS-based position and attitude estimation method presented in Section II relies on a strong assumption: that we precisely know the master-slave base vectors. This is however not always true in practice. In particular, suppose that the base vectors' lengths are subject to distorsions, then they write ${}_{\mathcal{B}}\mathbf{b}_{j,m} = (1+\delta_j){}_{\mathcal{B}}\widehat{\mathbf{b}}_{j,m}$, where ${}_{\mathcal{B}}\widehat{\mathbf{b}}_{j,m}$ is the assumed vector, and δ_j an unknown and unmodelled perturbation on the surveyed baseline to the j-th antenna. It turns out that it does not affect the position observation, as ${}_{\mathcal{B}}\mathbf{b}_{j,m}$ does not appear in (11). The components of the attitude observation $\mathbf{y}_{\text{att}}$, in (12), are however impacted, so that

$$\mathbf{y}_{\text{pos}} = \widehat{\mathbf{y}}_{\text{pos}} \tag{20}$$

$$[\boldsymbol{\Phi}_{j,m}]_i = [\widehat{\boldsymbol{\Phi}}_{j,m}]_i - \delta_j \mathbf{u}_i^\top \mathbf{R}(\mathbf{q}) {}_{\mathcal{B}}\widehat{\mathbf{b}}_{j,m} \tag{21}$$

$$[\boldsymbol{\rho}_{j,m}]_i = [\widehat{\boldsymbol{\rho}}_{j,m}]_i - \delta_j \mathbf{u}_i^\top \mathbf{R}(\mathbf{q}) {}_{\mathcal{B}}\widehat{\mathbf{b}}_{j,m}, \tag{22}$$

This mismatch is noticeable, because it is *linear* w.r.t. δ_j. Thus, the only approximation made in (16) is the use of $\widehat{\mathbf{q}}_{k|k-1}$, meaning that the quality of the Taylor expansion will only depend on the quality of the estimate. Indeed, the constraints which will be used for attitude or JPA estimation are given by

$$\boldsymbol{\Delta}_k^{\text{att}} = \begin{bmatrix} \mathbf{D}_1^{\text{att}} & \cdots & \mathbf{D}_N^{\text{att}} \end{bmatrix} \tag{23}$$

$$\boldsymbol{\Delta}_k^{\text{JPA}} = \begin{bmatrix} \mathbf{D}_1^{\text{JPA}} & \cdots & \mathbf{D}_N^{\text{JPA}} \end{bmatrix} \tag{24}$$

$$\mathbf{D}_j^{\text{att}} = \begin{bmatrix} \mathbf{0} \\ \vdots \\ \mathbf{U}\mathbf{R}(\widehat{\mathbf{q}}_{k|k-1}) {}_{\mathcal{B}}\widehat{\mathbf{b}}_{j,m} \\ \mathbf{0} \\ \vdots \\ \mathbf{U}\mathbf{R}(\widehat{\mathbf{q}}_{k|k-1}) {}_{\mathcal{B}}\widehat{\mathbf{b}}_{j,m} \end{bmatrix}, \quad \mathbf{D}_j^{\text{JPA}} = \begin{bmatrix} \mathbf{0} \\ \mathbf{D}_j^{\text{att}} \end{bmatrix} \tag{25}$$

where the non-zero block of $\mathbf{D}_j^{\text{att}}$ is located at the rows related to the j-th slave antenna, i.e. those of $\boldsymbol{\Phi}_{j,m}$ and $\boldsymbol{\rho}_{j,m}$. $\mathbf{U} \in \mathbb{R}^{n,3}$ is the matrix which stacks the steering vectors $\mathbf{u}_i^\top$. The obtained linearly constrained ESKF (LC-ESKF) for the attitude-only and JPA estimation is summarised in Algorithm 1

Algorithm 1: LC-ESKF algorithm for attitude-only and JPA in case of mismatched base vectors' lengths

Input: Prior $\mathbf{x}_0, \mathbf{C}_{\mathbf{x}_0}$, $({}_{\mathcal{B}}\widehat{\mathbf{b}}_{j,m})_m$;
Initialisation
  Set $\mathbf{P}_{0|0} = \mathbf{C}_{\mathbf{x}_0}, \mathbf{x}_{0|0} = \mathbf{x}_0$;
for $k \geq 1$ **do**
  Apply the process model in (7a)-(7b) to get $\mathbf{P}_{k|k-1}$ and $\mathbf{x}_{k|k-1}$;
  Compute the unconstrained gain $\mathbf{K}_k$, $\boldsymbol{\Delta}_k$, and the constrained gain $\mathbf{L}_k$ from (7d), (25) and (17) ;
  Compute $\mathbf{P}_{k|k}$ from (18)
  $\widehat{\mathbf{x}}_{k|k} = \widehat{\mathbf{x}}_{k|k-1} \oplus \mathbf{L}_k(\mathbf{y}_k - \mathbf{h}(\widehat{\mathbf{x}}_{k|k-1}, ({}_{\mathcal{B}}\widehat{\mathbf{b}}_{j,m})_m))$;
Output: $(\mathbf{x}_{k|k})_{k\geq 1}, (\mathbf{P}_{k|k})_{k\geq 1}$;

IV. Results

To assess both the sensitivity of JPA and attitude estimation to a mismatch on the base vectors, and the performance of the proposed linearly constrained filter to mitigate this mismatch, simulation experiments were carried out. We considered a medium-sized vehicle (e.g., a ship), containing 3 slave antennas in addition to the master one, and observing seven satellites (the sky plot coincides with [25]). Each slave antenna is assumed to be separated from the master antenna by a distance $\|{}_{\mathcal{B}}\widehat{\mathbf{b}}_{j,m}\| = 5$ m. The vehicle starts at a distance of 5 km from the base station, and its velocity follows a random walk, while its roll, pitch and yaw follow sine waves of amplitudes 0.1°, 3° and 180°, and of period 60 s, 10 s and 25 s, respectively. Constant length mismatches of 2 to 5% were considered for each master-slave vectors, i.e. $\delta_j \in [-0.05, 0.05]$. GNSS data was obtained at 1 Hz, and recorded for 100 s. The probability of cycle-slip was fixed at 0.5%. Stochastic modelling for the undifferenced GNSS observations follows a satellite elevation-dependent model [26], with the zenith-referenced code and carrier standard deviations given in Table I. Integer ambiguity resolution is performed via LAMBDA [27].

TABLE I
Monte Carlo simulation parameters.

Initial uncertainties standard deviations	Position: 10 [m], Velocity: 1 [(m/s)] Attitude: 10 [deg], Ambiguities: 5 [cycles] Gyroscope bias: 2.10^{-3} $[^\circ/\sqrt{s^3}]$
Process noise standard deviations	Gyroscope: 2.10^{-3} $[^\circ/\sqrt{s^3}]$ Bias random walk: 2.10^{-5} $[^\circ/(s\sqrt{s^3})]$ Velocity (East-North-Up): [1, 1, 10^{-3}] [m/s]
Observation noise standard deviations	Code zenith-referenced: 0.3 [m] Carrier phase zenith-referenced: 3 [mm]

The standard and linearly constrained versions of the attitude-only and the JPA ESKF filters were compared through 200 Monte Carlo runs. The latter are named LCAtt and LCJPA respectively. The root mean square error (RMSE) in position, attitude are displayed in Figure 2, along with the mean ambiguity success rate (MASR) –i.e., the average empirical success rate for the integer estimation over the Monte Carlo experiments–. Solutions before and after ambiguity resolution are presented, denoted "Float" and "Fix" respectively. It clearly appears that the mismatched lengths impact mostly the attitude and ambiguity estimations, and severely degrade them. Indeed, the Float position accuracy simply boils down to that of a single antenna, which does not depend on the mismatched vectors anymore. The failure in ambiguity resolution for standard JPA, however, happens to degrade its position accuracy, contrary to the LCJPA which reaches centimeter level. On the contrary, the constrained filters provide much better attitude estimates, and the advantage

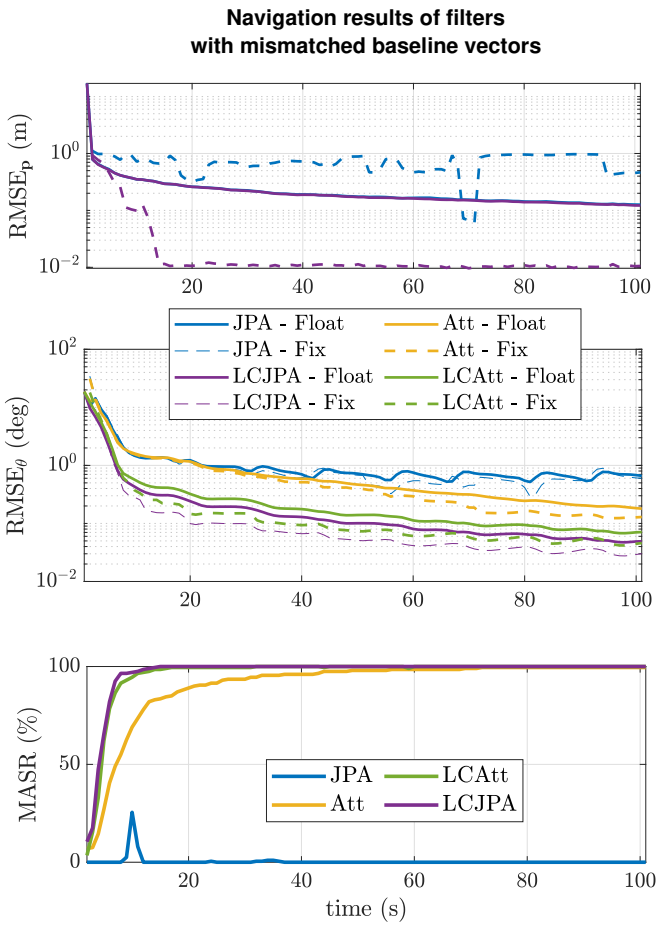

Fig. 2. Comparison of conventional and constrained filtering solutions for attitude-only and JPA problems under mismatched master-slave baseline lengths. Top: position RMSE over time. The Float solution accuracy is the same for JPA and LC-JPA, since the baseline mismatch does not directly impact the positioning. However, integer estimation on JPA induces biases due to the mismatch and its Fixed positioning is strongly degraded. Only the LCJPA takes advantage of the multi antennas to reach centimeter level error after ambiguity resolution. Middle: attitude RMSE. It clearly appears that the addition of constraints allows better performance. Moreover, LCJPA proves more accurate than attitude estimation only. Bottom: Mean ambiguity success rate (MASR). The standard JPA fails completely, explaining its degraded float results. Only the LCJPA and LCAtt quickly reach perfect ambiguity resolution.

of JPA over attitude-only estimation is clearly noticeable.

V. Conclusions

In this work, we studied how a mismatch on the master-slave antennas lengths can impact the accuracy of multi-antenna attitude-only and of the recently introduced joint position and attitude estimation. It turns out that a few percentages of error can lead to noticeable performance loss, in particular in the capability of JPA to correctly solve integer ambiguities. We proposed to leverage the framework of linearly constrained Kalman filtering to derive robust filters for these two problems. They proved to be able to mitigate this mismatch, and to recover the expected accuracy in a simulation experiment. The use of linear constraints thus offered an easy-to-implement and effective solution to maintain the filters' performance in the face of these mismatches, in a simulated environment. Future work will include validation of the proposed method on real data.

References

[1] P. J. G. Teunissen and O. Montenbruck, Eds., *Handbook of Global Navigation Satellite Systems*, Springer, Switzerland, 2017.

[2] V. W. Spinney, "Applications of the Global Positioning System as an Attitude Reference for Near Earth Users," *Navigation*, 1976.

[3] A. Hauschild, O. Montenbruck, and R. B. Langley, "Flight Results of GPS-Based Attitude Determination for the Canadian CASSIOPE Satellite," *Navigation*, vol. 67, no. 1, pp. 83–93, 2020.

[4] A. Hauschild, "GNSS Yaw Attitude Estimation: Results for the Japanese Quasi-Zenith Satellite System Block-II Satellites using Single-or Triple-Frequency Signals from Two Antennas," *Navigation*, vol. 66, no. 4, pp. 719–728, 2019.

[5] P. J. G. Teunissen, G. Giorgi, and P. J. Buist, "Testing of a New Single-Frequency GNSS Carrier Phase Attitude Determination Method: Land, Ship and Aircraft Experiments," *GPS Solutions*, vol. 15, no. 1, pp. 15–28, 2011.

[6] J. Schneider, C. Eling, L. Klingbeil, H. Kuhlmann, W. Förstner, and C. Stachniss, "Fast and Effective Online Pose Estimation and Mapping for UAVs," in *Proc. of the IEEE International Conference on Robotics and Automation (ICRA)*, 2016, pp. 4784–4791.

[7] L. Meyer et al., "The MADMAX Data Set for Visual-Inertial Rover Navigation on Mars," *Journal of Field Robotics*, March 2021.

[8] D. Medina, H. Li, J. Vilà-Valls, and P. Closas, "Robust Statistics for GNSS Positioning under Harsh Conditions: A Useful Tool?," *Sensors*, vol. 19, no. 24, pp. 5402, 2019.

[9] D. Medina, H. Li, J. Vilà-Valls, and P. Closas, "Robust Filtering Techniques for RTK Positioning in Harsh Propagation Environments," *Sensors*, vol. 21, no. 4, pp. 1250, 2021.

[10] P. J. G. Teunissen, "The Least-Squares Ambiguity Decorrelation Adjustment: A Method for Fast GPS Integer Ambiguity Estimation," *Journal of geodesy*, vol. 70, no. 1-2, pp. 65–82, 1995.

[11] P. J. G. Teunissen, "A General Multivariate Formulation of the Multi-Antenna GNSS Attitude Determination Problem," *Artificial Satellites*, vol. 42, no. 2, pp. 97–111, 2007.

[12] G. Giorgi, *GNSS Carrier Phase-Based Attitude Determination: Estimation and Applications*, Ph.D. thesis, TU Delft, 2011.

[13] D. Medina, J. Vilà-Valls, A. Heßelbarth, R. Ziebold, and J. García, "On the Recursive Joint Position and Attitude Determination in Multi-Antenna GNSS Platforms," *Remote Sensing*, vol. 12, no. 12, 2020.

[14] E. Hrustic, R. Ben Abdallah, J. Vilà-Valls, D. Vivet, G. Pagès, and E. Chaumette, "Robust linearly constrained extended kalman filter for mismatched nonlinear systems," *International Journal of Robust and Nonlinear Control*, vol. 31, no. 3, pp. 787–805, 2021.

[15] R. Ben Abdallah, J. Vilà-Valls, G. Pagès, D. Vivet, and E. Chaumette, "Robust LCEKF for Mismatched Nonlinear Systems with Non-Additive Noise/Inputs and Its Application to Robust Vehicle Navigation," *Sensors*, vol. 21, no. 6, pp. 2086, 2021.

[16] F. L. Markley, "Attitude Error Representations for Kalman Filtering," *Journal of Guidance, Control, and Dynamics*, vol. 26, no. 2, pp. 311–317, March 2003.

[17] J. L. Crassidis, F. L. Markley, and Y. Cheng, "Survey of nonlinear attitude estimation methods," *Journal of Guidance, Control, and Dynamics*, vol. 30, no. 1, pp. 12–28, 2007.

[18] T. D. Barfoot, *State Estimation for Robotics*, Cambridge University Press, 2017.

[19] S. I. Roumeliotis, G. S. Sukhatme, and G. A. Bekey, "Circumventing Dynamic Modeling: Evaluation of the Error-State Kalman Filter Applied to Mobile Robot Localization," in *Proc. of the IEEE International Conference on Robotics and Automation*, 1999, pp. 1656–1663 vol.2.

[20] J. Solà, "Quaternion Kinematics for the Error-State Kalman Filter," *CoRR*, vol. abs/1711.02508, 2017.

[21] J. Stillwell, *Naive Lie Theory*, Springer Sci. & Business Media, 2008.

[22] J. Sola, J. Deray, and D. Atchuthan, "A Micro Lie Theory for State Estimation in Robotics," *arXiv preprint arXiv:1812.01537*, 2018.

[23] Y. Bar-Shalom, X.-Rong Li, and T. Kirubarajan, *Estimation with Applications to Tracking and Navigation*, John Wiley & Sons, 2001.

[24] V. Passaro, A. Cuccovillo, L. Vaiani, M. De Carlo, and C. E. Campanella, "Gyroscope Technology and Applications: A Review in the Industrial Perspective," *Sensors*, vol. 17, no. 10, pp. 2284, 2017.

[25] D. Medina, J. Vilà-Valls, E. Chaumette, F. Vincent, and P. Closas, "Cramér-Rao Bound for a Mixture of Real- and Integer-Valued Parameter Vectors and Its Application to the Linear Regression Model," *Signal Processing*, vol. 179, 2021.

[26] H.-J. Eueler and C. C. Goad, "On Optimal Filtering of GPS Dual Frequency Observations Without Using Orbit Information," *Bulletin géodésique*, vol. 65, no. 2, pp. 130–143, 1991.

[27] P. De Jonge and C. C. J. M. Tiberius, *The LAMBDA Methods for Integer Ambiguity Estimation: Implementation Aspects*, vol. 12, Verlag der Delft Univers. of Technolog., 1996.